The preliminary analysis of the first dry-out in the helical coil tube

Yujeong Ko, Hyoung Kyu Cho*
Department of Nuclear Engineering, Seoul National Univ., 1 Gwanak-ro, Gwanak-gu, Seoul 08826
rhdbwjdo8o@snu.ac.kr
**Corresponding author: chohk@snu.ac.kr*

***Keywords : Helical coiled steam generator, i-SMR, Helical coil tube dry-out, First dry-out**

1. Introduction

Helical coiled steam generators are widely utilized in small modular reactors (SMRs) due to their compact design and enhanced heat transfer capabilities [1]. Therefore, helical coiled steam generators have been adopted in i-SMR [2] and SMART [3] in Korea. However, the unique geometric characteristics of helical coils introduce additional forces, leading to more complex heat transfer and dry-out phenomena compared to straight or U-tube steam generators.

Given the complexity of thermo-hydraulic phenomena within the helical coil tube, numerous studies have been conducted to investigate heat transfer and pressure drop [4,5]. This paper specifically focuses on examining the first dry-out phenomenon in helical coil tubes. In this paper, the appropriate first dry-out correlations have been selected and incorporated into the system code to conduct the preliminary simulations under normal operation conditions of i-SMR.

2. First dry-out in helical coil tube

2.1. Characteristics of the helical coil tube

The main characteristic of a helical coil tube is its curved and torsional geometry. This curved geometry causes the fluid to flow along a curved path, which induces centrifugal force within the fluid. The centrifugal force alters the velocity profile across the cross-sectional area, thereby generating a secondary flow force [6,7]. In the liquid phase, this secondary flow force changes the distribution of the liquid film along the circumferential direction, while in the gas phase, it influences both liquid droplet entrainment and redeposition [8]. Consequently, three forces—gravity (G), centrifugal force (C), and secondary flow force (S)—compete within the fluid in a helical coil tube, as illustrated in Fig. 1. These competing forces result in an asymmetric liquid film distribution, as shown in Fig. 2 [9]. This leads to local dry-out at specific locations, a phenomenon known as the first dry-out. Along the axial direction, dry-out progresses, creating a region known as partial dry-out. Eventually, the liquid film disappears entirely, leading to what is called total dry-out. The most significant difference compared to straight tubes is the presence of an extended partial dry-out region. Therefore, it is crucial for system codes to account for these distinct phenomena by identifying the first and total dry-out.

As the first dry-out occurs, the liquid film distribution changes based on the dominance of competing forces. To categorize the effects of these forces, Berthoud and Jayanti [9] proposed a first dry-out dominance map, depicted in Fig. 3. The region where gravity dominates is termed the gravity zone, the region dominated by secondary flow is called the redeposition zone, and the region where centrifugal force dominates is referred to as the entrainment zone. This map was later modified by Hwang et al. [10], specifically in the boundary between the gravity and redeposition zones.

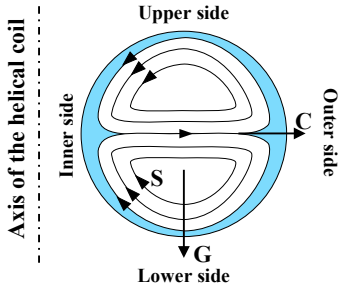

Fig. 1. Competing forces applied in a fluid of helical coil tube

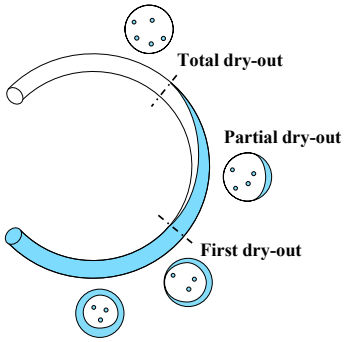

Fig. 2. Dry-out progress in helical coil tube

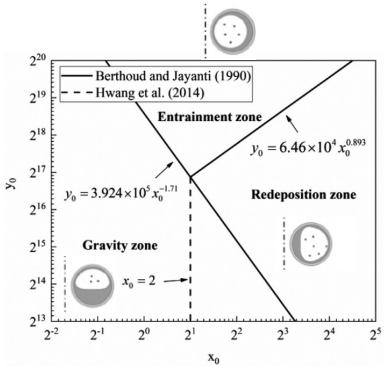

Fig. 3. First dry-out dominance map for helical coil tube [7,8]

2.2. The first dry-out quality correlations

The correlations for predicting the first dry-out quality were derived from heuristic experimental results. Berthoud and Jayanti [7] and Xu et al. [9] proposed correlations specific to each of the three dominance zones. Кутателадзе et al. [10] categorized correlations based on the external diameter of the helical coil tube, while Mao et al. [11] classified according to the mass flux condition. Santini et al. [12] and others validated these correlations within the specific conditions of their experiments.

Berthoud correlation [7]

- Gravity zone

(1) $x_1 = 10^{7.068}\left(\frac{\rho_f}{\rho_g}\right)^{-2.378}\left(\frac{Gd_i}{\mu_l}\right)^{-1.712}\left(\frac{G}{\rho_g\sqrt{gD}}\right)^{0.967}\left(\frac{Q}{GH_{fg}}\right)^{-0.740}$

- Redeposition zone

(2) $x_1 = 3.223 + \log_{10}\left(\left(\frac{\rho_f}{\rho_g}\right)^{0.101}\left(\frac{Gd_i}{\mu_l}\right)^{-0.785}\left(\frac{G}{\rho_g\sqrt{gD}}\right)^{0.067}\left(\frac{Q}{GH_{fg}}\right)^{-0.430}\left(\frac{Q}{\mu_l H_{fg}}\sqrt{\frac{\sigma}{g(\rho_l-\rho_v)}}\right)^{0.098}\right)$

- Entrainment zone

(3) $x_1 = 10^{3.235}\left(\frac{\rho_f}{\rho_g}\right)^{-0.267}\left(\frac{Gd_i}{\mu_l}\right)^{-0.984}\left(\frac{G}{\rho_g\sqrt{gD}}\right)^{0.950}\left(\frac{Q}{GH_{fg}}\right)^{-0.428}\left(\frac{Q}{\mu_l H_{fg}}\sqrt{\frac{\sigma}{g(\rho_l-\rho_v)}}\right)^{0.119}$

Xu correlation [9]

- Gravity zone

(4) $x_1 = 29.81\left(\frac{\rho_f}{\rho_g}\right)^{0.417}\left(\frac{G}{\rho_g\sqrt{gD}}\right)^{-0.122}[1-\exp(-0.0011 + Bo)]\left(\frac{gQd^4}{k_f\mu_g^2}\frac{\rho_f-\rho_g}{\rho_f T_{sat}}\right)^{0.1769}$

- Redeposition zone

(5) $x_1 = 1 - 5.287\cdot 10^7\left(\frac{\rho_f}{\rho_g}\right)^{-0.7953}\left(\frac{G}{\rho_g\sqrt{gD}}\right)^{0.3108}Bo^{1.5296}\left(\frac{gQd^4}{k_f\mu_g^2}\frac{\rho_f-\rho_g}{\rho_f T_{sat}}\right)^{-0.4180}\left(\frac{d}{D}\right)^{-0.1228}$

- Entrainment zone

(6) $x_1 = 439.3\left(\frac{\rho_f}{\rho_g}\right)^{0.105}\left(\frac{Gd_i}{\mu_l}\right)^{-0.984}[1-\exp(-8.27\cdot 10^{-4} + Bo)]\left(\frac{gQd^4}{k_f\mu_g^2}\frac{\rho_f-\rho_g}{\rho_f T_{sat}}\right)^{0.0614}$

Кутателадзе correlation [10]

(7) $x_1 = \begin{cases}0.3 + 0.7e^{-45\omega} & for\ d_e \le 0.008\\ (0.3 + 0.7e^{-45\omega})\left(\frac{0.008}{d_e}\right)^{0.15} & for\ d_e > 0.008\end{cases}$

Mao correlation [11]

(9) $x_1 = \begin{cases}0.052Bo^{-0.208}Re_g^{0.071}\left(\frac{\rho_f}{\rho_g}\right)^{0.110} & for\ G < 1000k\,g/m^2\,s\\ 450Bo^{-0.225}Re_g^{-0.651}\left(\frac{\rho_f}{\rho_g}\right)^{0.226} & for\ G \ge 1000k\,g/m^2\,s\end{cases}$

Santini correlation [12]

(8) $x_1 = 0.44 - 0.0006e - 5P\cdot G^{0.114}$

2.2. Implementation of first dry-out quality correlations

Several experiments were selected to implement the first dry-out quality correlations. The experimental conditions are plotted on the dry-out dominance map as shown in Fig. 4.

Using the data from these selected experimental conditions, the first dry-out quality correlations introduced in Section 2.2 were applied. The results of the comparison between the experimental data and the calculated first dry-out quality using each correlation are summarized in Fig.5. Overall, Кутателадзе correlation performed well across all regions.

More specifically, comparisons were made within each dominant region using dry-out dominance maps proposed by Berthoud and Hwang, as shown in Table 1. Based on the calculated RMS errors in each dominant region, the modified dry-out dominant map introduced by Hwang et al. [8] was selected. For each dominant region, the Santini correlation was chosen for the gravity zone, the Кутателадзе correlation for the redeposition zone, and the Berthoud correlation for the entrainment zone. The results using different correlations for each zone are depicted in Fig. 6, showing better predictions with the modified dominance map.

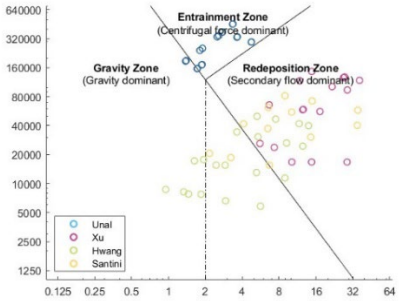

Fig. 4. The dry-out dominance map of each experimental condition

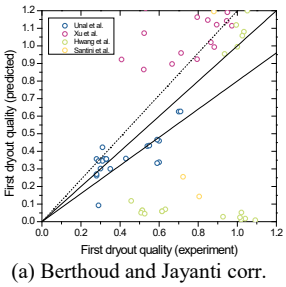

(a) Berthoud and Jayanti corr.

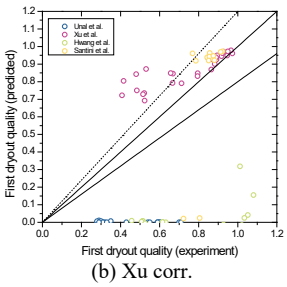

(b) Xu corr.

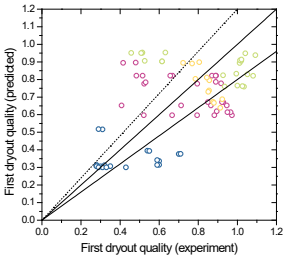

(c) Кутателадзе corr.

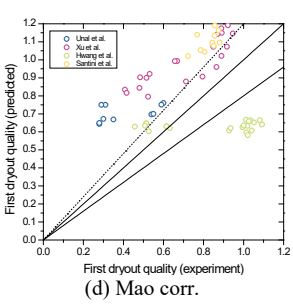

(d) Mao corr.

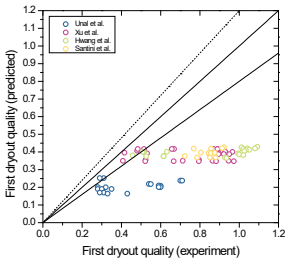

(e) Santini corr.

Fig. 5. Comparison of first dry-out quality between experimental results and calculated result using each correlation

Table 1. RMS error using each correlation in each zone

Zone	Berthoud corr.	Xu corr.	Кутателадзе corr.	Mao corr.	Santini corr.
Berthoud map					
Gravity	0.358	0.446	0.227	0.307	**0.194**
Redeposition	0.398	0.241	**0.155**	3.70e6	0.231
Entrainment	**0.106**	0.447	0.157	1.49e7	0.246
Hwang et al. map					
Gravity	0.320	0.441	0.284	0.365	**0.139**
Redeposition	0.400	0.282	**0.145**	3.42e6	0.235
Entrainment	**0.106**	0.447	0.157	1.49e7	0.246

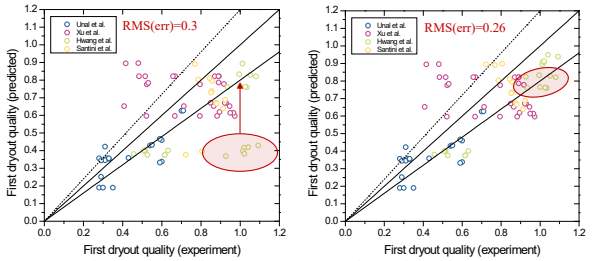

(a) Using Berthoud map (b) Using Hwang map

Fig. 6. Comparison of first dry-out quality adopting selected correlation for each dominance zone

3. Helical coil model in system code MARS-KS

3.1. Heat transfer model for the helical coil in MARS-KS

To implement the first dry-out phenomenon into the system code MARS-KS, the heat transfer mode determination mechanism for the helical coil model was reviewed. The existing method, shown in Fig. 7-(a), determines the dry-out and single-phase conditions based on specific void fraction values. However, due to the wide variation in quality within the high void fraction region, a determination condition based on quality is necessary. Therefore, the mechanism was modified to incorporate equilibrium quality, as illustrated in Fig. 7-(b).

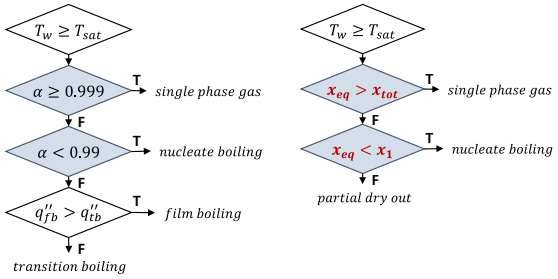

(a) Before modification (b) After modification

Fig. 7. Heat transfer mode determination mechanism for helical coil tube model in MARS-KS

3.2. Nodalization of i-SMR helical coil tube part

A simplified simulation was conducted under the normal operation conditions of the i-SMR. The simulation was calculated for the tube side (secondary side) of the helical coiled steam generator. Heat flux was gradually increased in steps to observe the entire boiling region. The nodalization is depicted in Fig. 8. Four conditions were selected for comparison; a straight tube, a helical coil with the default heat transfer mod (HTM) model, a helical coil with the first dry-out HTM model, a helical coil with the first and last dry-out determination HTM models.

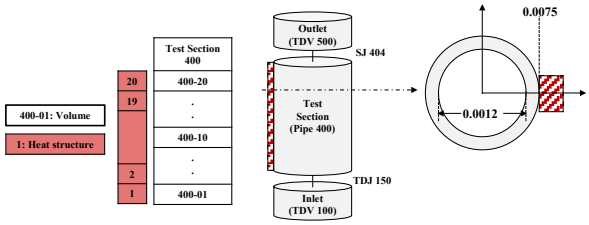

Fig. 8. Nodalization of simplified i-SMR helical coiled steam generator (tube side)

3.3. Result of heat transfer in helical coil tube model

The simulation results under normal operation conditions, with a superheated temperature of 30 K, are summarized in Fig. 9. As shown in Fig. 9-(a), the straight tube model predicted that dry-out occurs earlier than in the helical model, leading to a higher wall temperature, as depicted in Fig.9-(b). When comparing the helical coil models with different HTM determination methods, dry-out occurs earlier in the model using the first dry-out HTM methods (red and pink lines) compared to the default model (gray line).

The simulations were repeated under reduced mass flux conditions, at 75% and 50% of the normal operation condition. The results are summarized in Fig. 10. As shown in Fig. 10-(c), dry-out could occur at a low-quality condition, which shows a significant difference from the default model.

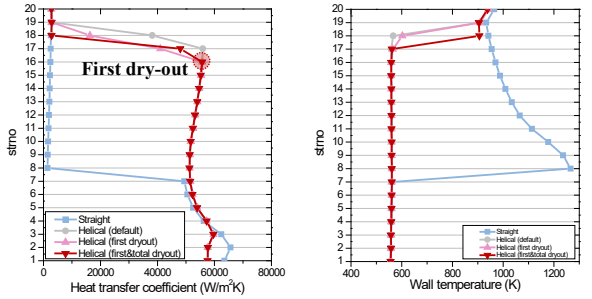

(a) Heat transfer coefficient (b) Wall temperature

Fig. 9. The distribution in the tube at a superheated temperature of 30 K under normal operation conditions

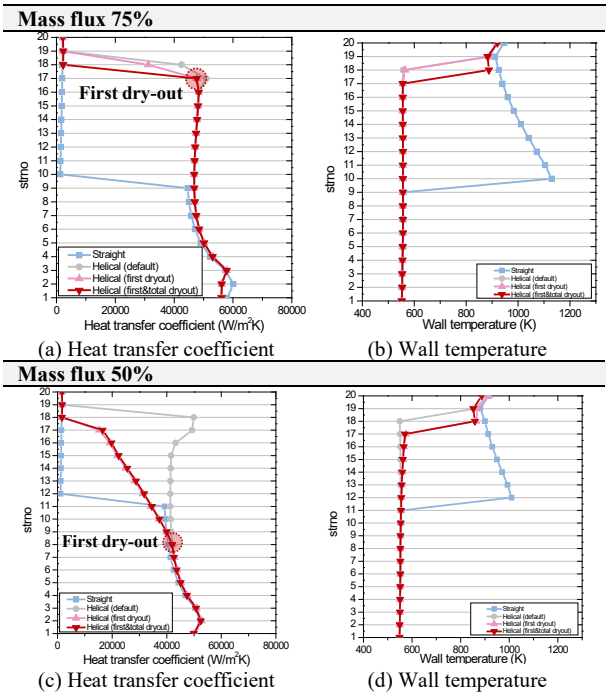

(a) Heat transfer coefficient (b) Wall temperature

(c) Heat transfer coefficient (d) Wall temperature

Fig. 10. The distribution in the tube at a superheated temperature of 30 K under reduced mass flux conditions

4. Conclusion

Helical coiled steam generators are widely adopted in small modular reactors due to their compact design and enhanced heat transfer capabilities. However, the boiling process in helical coil tubes differ from that in straight tubes due to their unique geometric characteristics. To better represent the actual physics of helical coil tubes in the system code MARS-KS, the heat transfer mode determination mechanism was modified to use quality values instead of void fraction. As a result, the dry-out occurrence point varied with changes in fluid conditions, particularly under low mass flux conditions. These simplified preliminary simulations highlight the necessity to modify the heat transfer mode for the helical coil tube models. In future studies, simulations will be conducted on both the tube and shell sides using the same heat transfer mode determination strategy.

ACKNOWLEDGEMENT

This work was supported by the Innovative Small Modular Reactor Development Agency grant funded by the Korea Government(MSIT) (No. RS-2024-00408520).

REFERENCES

[1] Cinotti, L., Bruzzone, M., Meda, N., Corsini, G., Lombardi, C. V., Ricotti, M., & Conway, L. E. (2002, January). Steam generator of the international reactor innovative and secure. In International Conference on Nuclear Engineering (Vol. 35960, pp. 983-990).

[2] Current Status of i-SMR Development and Deployment, Nuclear Safety & Security Information Conference 2021, 2021

[3] KAERI, 2023. Innovative Growth and Job Creation https://www.kaeri.re.kr/board?menuId=MENU00725

[4] Chung, Y. J., Bae, K. H., Kim, K. K., & Lee, W. J. (2014). Boiling heat transfer and dryout in helically coiled tubes under different pressure conditions. Annals of Nuclear Energy, 71, 298-303.

[5] Hardik, B. K., & Prabhu, S. V. (2017). Critical heat flux in helical coils at low pressure. Applied Thermal Engineering, 112, 1223-1239.

[6]Dean, W. R., & Hurst, J. M. (1959). Note on the motion of fluid in a curved pipe. Mathematika, 6(1), 77-85.

[5] Dravid, A. N., Smith, K. A., Merrill, E. W., & Brian, P. L. T. (1971). Effect of secondary fluid motion on laminar flow heat transfer in helically coiled tubes. AIChE Journal, 17(5), 1114-1122.

[6] Ishida, K. (1981). Two-phase flow with heat transfer in helically-coiled tubes (Doctoral dissertation, Department of Civil and Mechanical Engineering, Imperial College London).

[7] Berthoud, G., & Jayanti, S. (1990). Characterization of dryout in helical coils. International journal of heat and mass transfer, 33(7), 1451-1463.

[8] Hwang, K. W., Kim, D. E., Yang, K. H., Kim, J. M., Kim, M. H., & Park, H. S. (2014). Experimental study of flow boiling heat transfer and dryout characteristics at low mass flux in helically-coiled tubes. Nuclear Engineering and Design, 273, 529-541.

[9] Xu, Z., Liu, M., Chen, C., Xiao, Y., & Gu, H. (2022). Development of an analytical model for the dryout characteristic in helically coiled tubes. International Journal of Heat and Mass Transfer, 186, 122423.

[10] Ge-Ping, W. U., Sui-Zheng, Q. I. U., Guang-Hui, S. U., Dou-Nan, J. I. A., & Dong-Hua, L. U. (2006). Experimental research on dryout point of flow boiling in narrow annular channels. Nuclear Science and Techniques, 17(4), 252-256.

[11] Mao, Y., Guo, L., Bai, B., Zhen, F. Q., & Guo, M. (2011). Experimental investigation on the dryout point for two-phase flow boiling of steam-water at high pressures in helical coils. Journal of Engineer-ing Thermophysics, 32(7), 1.

[12] Santini, L., Cioncolini, A., Lombardi, C., & Ricotti, M. (2014). Dryout occurrence in a helically coiled steam generator for nuclear power application. In EPJ Web of Conferences (Vol. 67, p. 02102). EDP Sciences.